Vacuum 85 (2011) 792–797

Contents lists available at ScienceDirect

Vacuum

journal homepage: www.elsevier.com/locate/vacuum

Microstructure and property evolution of Cr-DLC films with different Cr content deposited by a hybrid beam technique

Wei Dai, Peiling Ke, Aiying Wang*

Division of Surface Engineering, Ningbo Institute of Materials Technology and Engineering, Chinese Academy of Sciences, Ningbo, China

ARTICLE INFO

Article history:
Received 17 September 2010
Received in revised form
11 November 2010
Accepted 16 November 2010

Keywords:
Diamond-like carbon
Microstructure
Surface morphology
Mechanical property

ABSTRACT

Cr-containing diamond-like carbon (Cr-DLC) films was deposited on silicon wafers by a hybrid beams system, which consists of a DC magnetron sputtering and a linear ion source. The chromium content in the films was adjusted by varying the fraction of Ar in the Ar and CH_4 gas mixture. The composition, microstructure, surface morphology, mechanical properties and tribological behavior of the films were investigated by XPS, TEM, AFM, SEM, nano-indentation and tribological tester as a function of Cr content. It is shown that, as the Cr content increased from 1.49 to 40.11 at.%, the Cr-DLC films transfer from amorphous DLC with dispersed metallic-like Cr to composite DLC with carbide phases embedding in the DLC matrix, and the film surface morphology also evolve from flat surface into rough surface with larger hillocks. The amorphous Cr-DLC films exhibit a low friction coefficient and wear rate as pure DLC, while the composite Cr-DLC films show a higher friction coefficient and wear rate, although they possess a relatively high hardness.

1. Introduction

In recent years, numerous metallic elements (e.g. Cr, Ti, W, Ag, and Cu) have been attempted to overcome the shortcomings of diamond-like carbon (DLC) films such as high residual stress, poor thermal stability and ductility [1–5]. Among those doping metals, carbide former, like Cr [6], Ti [7], and W [3], can exist as either metallic cluster dissolving in DLC films or metal carbide phase embedding in the amorphous carbon matrix, which will significantly influence the mechanical and tribological properties. Singh et al. [6] studied Cr-containing DLC (Cr-DLC) films by a hybrid PVD/PECVD process and found that Cr-DLC films with low Cr content had similar microstructure and tribological characteristics with those of pure DLC films, while the films with high Cr content exhibited a composite structure with carbide phase embedding in the DLC phase and thus the tribological behavior of the films was characterized by abrasive wear. The formation of the carbide phase is expected to depend on the doped metal solubility in the DLC matrix, which significantly correlates with the deposition technique and the process parameter. Zhang and co-workers [2] deposited Ti-DLC films using co-sputtering of graphite and titanium targets. Nanocrystalline of TiC was detected in amorphous matrix of a-C when the Ti content was increased to 16 at.%. In another work, Meng et al. [7] reported that the dissolution limit of Ti atoms in the DLC films deposited by reactive magnetron sputter technique was between 0.9 and 2.5 at.%. Beyond this dissolution limit, nanocrystalline could be observed in the films.

The purpose of the present paper was to report the results of experiments designed to prepare Cr-DLC films using a hybrid beams system comprising an anode-layer linear ion beam source and a DC magnetron sputtering unit. The composition and microstructure evolution of the films were studied as a function of the Cr content. The film surface morphology, mechanical property and tribological behavior were discussed according to the composition and microstructure of the films with various Cr contents.

2. Experimental details

Silicon (100) wafers of thickness at 525 ± 15 μm were used as the substrates, which were cleaned ultrasonically in acetone, ethanol, and dried in air before being put into the vacuum chamber. The Cr-DLC films were prepared by a hybrid beams system, which consists of a DC magnetron sputtering and a linear ion source (LIS) [8]. The substrates were biased by an asymmetrically bipolar pulsed power (Pinnacle Plus 5 kW, Advanced Energy), which would supply a square wave pulsed bias with a frequency of 350 kHz and a reversal time of 1.1 μs. Prior to deposition, the substrates were sputter-cleaned for 10 min using Ar ions at a bias voltage of −100 V. The base pressure was evacuated to the vacuum of 2.5×10^{-5} bar. During depositing process, the work pressure was kept at about 4.4×10^{-3} bar. CH_4 gas was

* Corresponding author.
E-mail address: aywang@nimte.ac.cn (A. Wang).

0042-207X/$ – see front matter © 2010 Elsevier Ltd. All rights reserved.
doi:10.1016/j.vacuum.2010.11.013

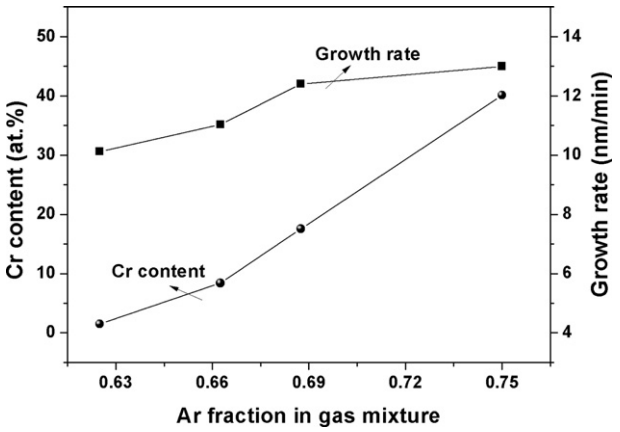

Fig. 1. Cr content and growth rate of the films as a function of Ar fraction in Ar and CH_4 gas mixture.

introduced into the LIS to obtain the hydrocarbon ions beam. Ar gas was supplied to the magnetron sputtering to sputter Cr target. The content of chromium atoms in the films was controlled by varying the gas fraction of Ar in the precursor gases and the total gas flux (Ar and CH_4) was kept at 80 sccm. Typical value of LIS voltage and current were 1200 ± 50 V and 0.2 A (current model), respectively. The DC power supplied to the sputtering gun was about 950 W (2.5 A)

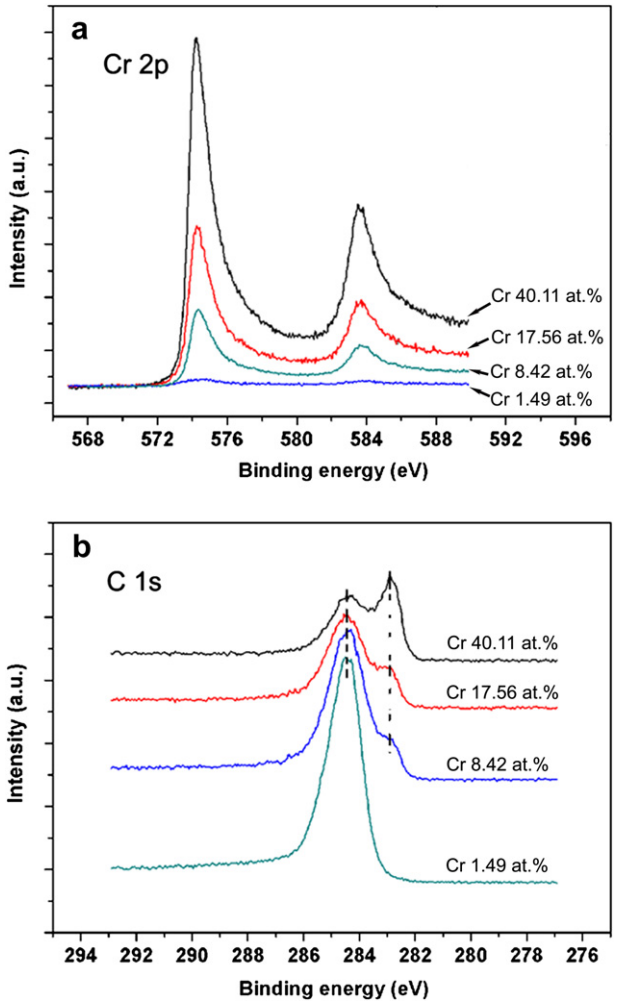

Fig. 2. Typical high-resolution XPS spectra of the films with different Cr content: (a) Cr 2p core level peak and (b) C 1s core level peak.

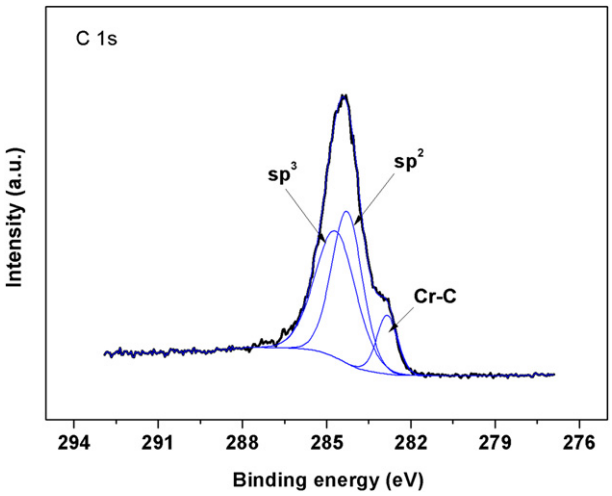

Fig. 3. Deconvolution of the XPS C 1s peak of the film with 8.42 at.% Cr.

(current model). A bias voltage of −50 V was applied to the substrate. The deposition time was 1 h.

The thicknesses of the deposited films were measured by a cross-section SEM (S-4800, Hitachi, Japan) measuring scale, and the film thicknesses are ranging from 600 nm to 780 nm. An X-ray photoelectron spectroscopy (XPS, Axis ultradld, Japan) with Al (mono) Kα irradiation at a pass energy of 160 eV was used to characterize the chemical composition and chemical bonds of the deposited films. The XPS energy step size was 0.05 eV for the high-resolution spectrums. Before commencing the measurement, Ar^+ ion beam with the energy of 3 keV was used to etch the sample surface for 5 min to remove contaminants. High-resolution transmission electron microscopy of the films was performed on Tecnai F20 electron microscope operated at 200 keV with a point-to-point resolution of 0.24 nm. The TEM specimen was prepared by peeling off the film from the NaCl crystalline substrate, which was dissolved in deionized water. The surface morphology of the films was studied by SPM (Dimension 3100 V, Veeco, US) at a scan rate of 1.5 Hz. The root-mean-square (RSM) roughness R_q of the film surfaces was calculated from 512 × 512 surface height data points obtained from 1 μm × 1 μm scan area [9]. Mechanical properties were measured by the nano-indentation technique in a continuous stiffness measurement (CSM) mode with a maximum indentation

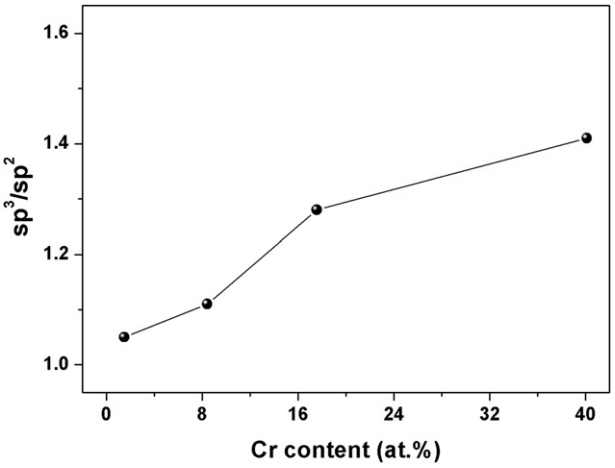

Fig. 4. The sp^3/sp^2 ratio determined from fitting the XPS C 1s peak as a function of Cr content.

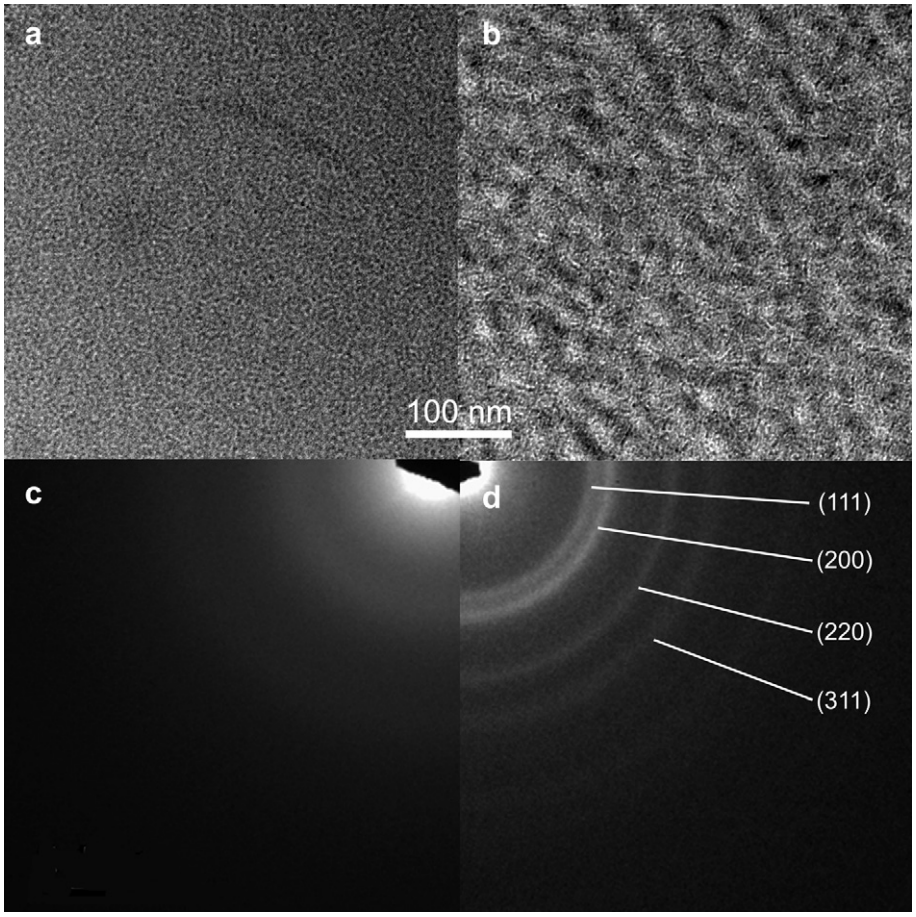

Fig. 5. TEM micrograph and corresponding diffraction pattern of the Cr-DLC films with (a) and (c) 8.42 at.%, and (b) and (d) 40.11 at.% Cr.

depth of 500 nm. The characteristic hardness of the films was chosen in the depth around 1/10th of the film thickness to minimize the substrate contribution. Six replicate indentations were made for each sample. The tribological behaviors of the films were tested on a rotary ball-on-disk tribometer at room temperature with a relative humidity of 40–50% under dry sliding conditions. A steel ball (SUJ-2, HRC60) with a diameter at 7 mm was used as the friction counter body. All the tests were performed at 0.1 m s^{-1} sliding velocity for a distance of 300 m and the applied load was 3 N. After the friction test, the wear traces were observed by a 3D scanning surface profiler (AEP, US).

3. Results and discussion

Fig. 1 shows the Cr content and growth rate of the films as a function of the Ar fraction. The Cr/C atomic ratio of the films was

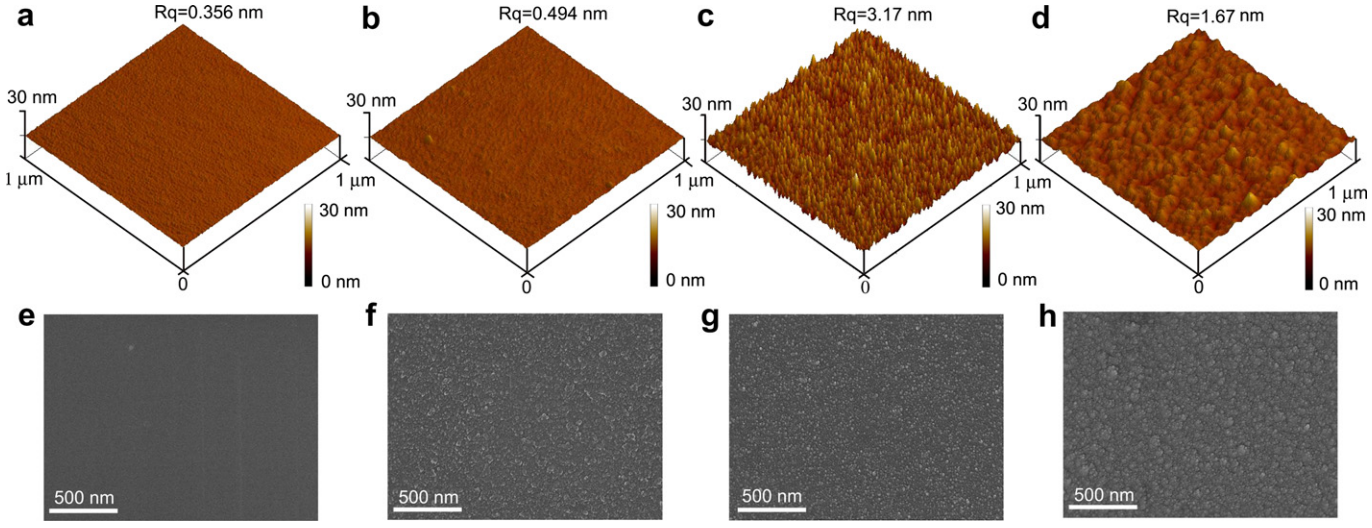

Fig. 6. AFM (upper) and SEM (lower) images of the Cr-DLC films with (a) and (e) 1.49 at.%, (b) and (f) 8.42 at.%, (c) and (g) 17.56 at.%, and (d) and (h) 40.11 at.% Cr.

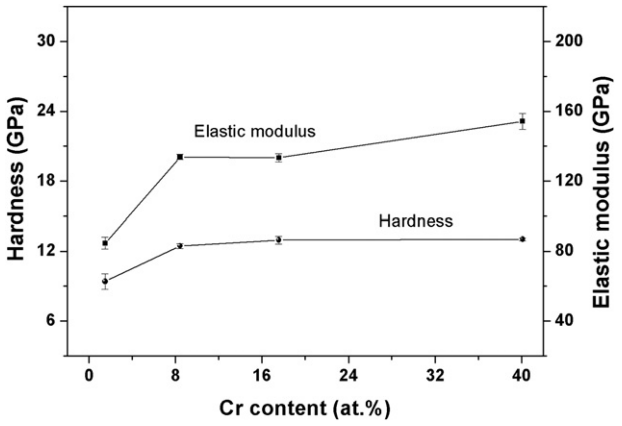

Fig. 7. Hardness and elastic modulus of the Cr-DLC films with various Cr contents.

determined based on the atomic sensitivity factors and area ratio of the C 1s to Cr 2p peaks in XPS spectra of the films (Hydrogen atom content was not considered due to its signal intensity below the XPS detection threshold). As the Ar fraction increases, the Cr content increases monotonically. This indicates that the chromium content in the films can be adjusted by varying the Ar fraction in the gas mixture. The growth rate of the films also increases with increasing Ar fraction, implying that the Cr doping would improve the growth rate of the films deposited by the hybrid beams.

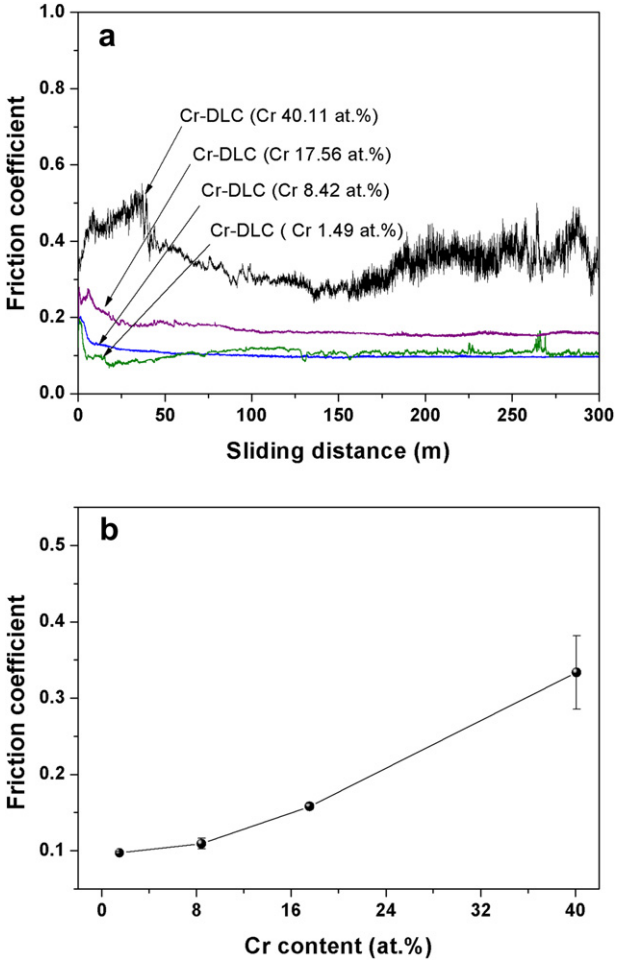

Fig. 8. Friction coefficient of the Cr-DLC films as a function of sliding distance.

The chemical bonds of the deposited films were detected by the XPS spectra. Fig. 2 shows the high-resolution Cr 2p and C 1s core level XPS spectra of the Cr-DLC film with various Cr contents. The Cr 2p spectra reveal a major peak at a binding energy around 574 eV and the presence of a shoulder around 583.7 eV in all spectra. The intensity of the Cr 2p peak increases with increasing Cr content. However, there is no significant difference between the Cr 2p peaks in those Cr-DLC films. In fact, the Cr 2p peak could not be used effectively to differentiate the chemical bonds between metallic Cr and Cr carbide. Nevertheless, the C 1s spectrum can be use to determine the films chemical state. The C 1s spectrum of the film with Cr 1.49 at.% only reveals a single peak around 284.5 eV, which originates from C–C or C–H bonding in DLC phase [6]. As the Cr content increases, a shoulder peak appears at a lower binding energy of about 283 eV, which can be assigned to carbon in carbide state [10]. This demonstrates that the carbide is formed in the films. The intensity of the peak sharply increases with the Cr content increased, implying that the fraction of chromium carbide increased since the intensity of the C 1s shoulder peak is an indication of the chromium carbide content in the films.

Further analysis of the C 1s XPS spectra can be acquired in the peaks deconvolution results [11]. Normally, the C 1s spectra can be deconvoluted into three components around 283 eV, 284.2 eV and 284.7 eV, corresponding to Cr–C, sp^2–C and sp^3–C, respectively (see Fig. 3). Subsequently, the ratio of sp^3/sp^2 carbon atoms in the films is determined as the ratio of the corresponding sp^3 peak area over the sp^2–C 1s peak area. Fig. 4 presents the sp^3/sp^2 ratio as a function of Cr content. It should be noted that the sp^3/sp^2 ratio increases monotonously with increasing the Cr content. Since sp^2–C has the relative lower bonding energy than sp^3–C, it would favor to bond with the Cr atoms to form the carbide phase. Consequently, as Cr content increases, a larger number of sp^2–C are used to formed carbide phase and thus results in the decrease of sp^2–C fraction and the increase of the sp^3/sp^2 ratio.

Fig. 5 shows the typical TEM micrograph and corresponding diffraction pattern of the films with 8.42 and 40.11 at.% Cr. At a small amount of Cr content at 8.42 at.%, as shown in Fig. 5(c), the ring-like in the diffraction pattern indicates that the crystal phases begin to evolve in the amorphous carbon matrix. However, the crystalline phase has not been observed in the plan-view image (Fig. 5(a)) yet due to the low Cr content. Further increasing the Cr content to 40.11 at.%, a granular nanocomposite structure with the uniform nano-scale particle-like embedded into the amorphous carbon matrix is observed (Fig. 5(b)). However, the exact size and configuration of particles are rather hard to be deduced because of the present limited TEM resolution. The distinct rings displayed in the diffraction patterns (Fig. 5(d)) are identified to be the (111), (200), (220) and (311) reflections of the face-centered (FCC) chromium carbide crystal. The lattice distance is simulated around 0.41 nm, which might be attributed to the metastable B1-CrC crystal phase [12]. The TEM results indicate that the Cr-DLC film with low Cr content doping should be the amorphous DLC with dispersed metallic-like Cr, while the film with high Cr content doping present as the composite DLC with carbide phases embedding in the DLC matrix.

Fig. 6 shows the images of AFM and SEM of the films with different Cr content. The Cr-DLC film with 1.49 at.% Cr is characterized by a low RMS roughness of 0.356 nm, and appear smooth for AFM and SEM images. As Cr content increases up to 17.56 at. %, the roughness of the film increases to 3.17 nm. The AFM morphology of the film with 17.56 at.% Cr shows numerous hillocks on the surface and the corresponding SEM image also reveal many granular contrasts. This implies that the films with low Cr content doping mainly exhibit the feature of the amorphous DLC with

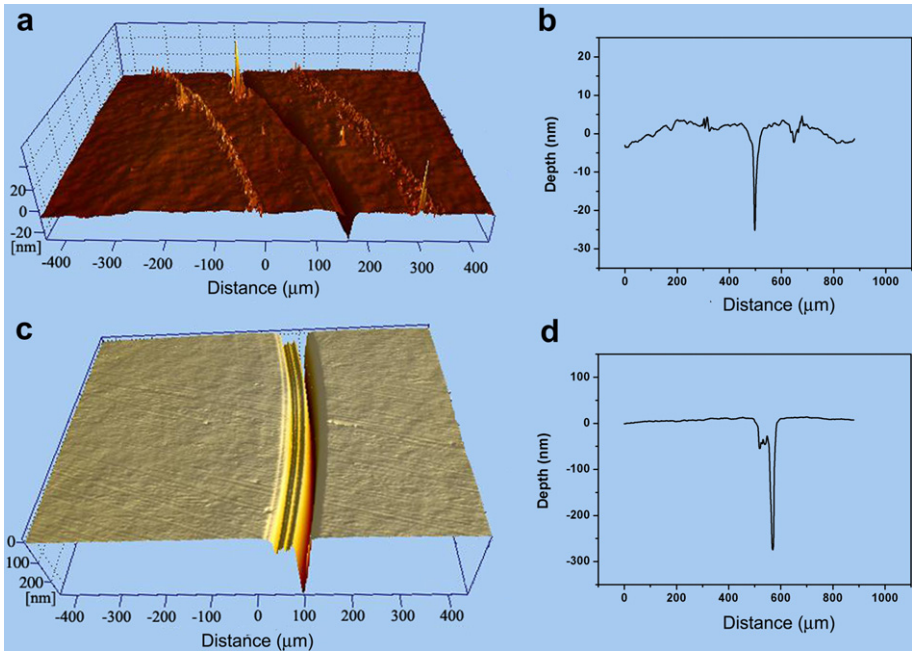

Fig. 9. Wear tracks micrograph and corresponding cross-section profiles of the films: (a) and (b) 1.49 at.%, and (c) and (d) 40.11 at.% Cr after friction test.

dispersed metallic-like Cr, and thus possess a smooth surface. When the Cr content of the films increases up to 17.56 at.%, a large amount of chromium carbide phase are formed in the films, which have been expected to increase the film surface roughness [13]. However, as the Cr content increases to 40.11 at. %, in spite of higher metallic content, the RMS roughness of the films dramatically decreases to 1.67 nm. The AFM micrograph of the film shows that the surface hillocks seem to be merged into bigger agglomerates appearing larger bumps, which may cause the film surface roughness to decrease.

The hardness and elastic modulus of the Cr-DLC films are presented in Fig. 7. It should be noted that there is an increase in the hardness of the Cr-DLC films followed by stabilization of hardness around 12 GPa. The initial increase of the hardness mainly originates the formation of the hard carbide phase, which will enhance the mechanical hardness of the films [6]. Furthermore, the increase of the sp^3/sp^2 ratio also contributes to the hardness increase. However, as incorporation of more Cr atoms ($\geq$8.42 at.%), a large amount of carbide phases will break the continuity of the carbon network and thus cause the hardness to decrease. Accordingly, these counteracting factors result in the relatively stable hardness at high Cr content (>1.49 at.%).

Fig. 8 shows the friction coefficient evolution of the Cr-DLC films with sliding distance. It can be seen that the Cr-DLC films containing low Cr atoms ($\leq$8.42 at.%) present a low friction coefficient of about 0.15. As the Cr content increases, the friction coefficient of the films increases sharply. When the Cr content reaches up to 40.11 at.%, the film shows a high friction coefficient of about 0.3 and performs a non-stable friction behavior with continuous oscillatory peaks in the friction coefficient. This can be attributed to the presence of hard chromium carbide phase, which has been expected to increase friction [14].

Fig. 9 reveals the typical wear tracks micrograph and corresponding cross-section profiles of the films with 1.49 and 17.56 at.% Cr after friction test. The Cr-DLC film with 1.49 at.% Cr (Fig. 9(a)) shows a smooth wear track with the low wear depth of about 25 nm. The wear rate of the film is about 8.9×10^{-9} mm^3/N-m. However, the wear depth sharply increases to about 280 nm in the film with 17.56 at.% Cr, as shown in Fig. 9(b), and the wear rate increases to 1.4×10^{-7} mm^3/N-m dramatically. The friction and wear behaviors of the Cr-DLC films mainly correlate with the composition and microstructure of the Cr-DLC films. At low Cr content, the films exhibit the feature of amorphous DLC with a small amount of Cr atoms dispersed in it. Thus, the films present a low friction coefficient and high wear resistance as pure DLC films [14]. While at high doping, the films are composite Cr-DLC consisting of the chromium carbide phase embedding in DLC. The hard carbide phase has been expected to cause abrasive wear, and thus increase wear. So the films show a high friction coefficient and larger wear depth.

4. Conclusions

The Cr-DLC films were deposited by the hybrid beams hybrid beam source, which consists of a DC magnetron sputtering unit and a linear ion source. The Cr content of the films could be varied from 1.49 to 40.11 at.% by adjusting Ar fraction in the Ar and CH_4 gas mixture. It is shown that the dissolution limit of Cr atoms in the DLC matrix deposited by the hybrid beam technique is around 8.42 at.%. The films with less than 8.42 at.% Cr exhibit the feature of the amorphous DLC structure with dispersed metallic-like Cr, which reveal a smooth surface, low friction coefficient and wear rate as the pure DLC. Above the content of about 8.42 at.%, a larger amount of carbide phase is formed and the films evolved into the composite DLC films with carbide phases embedding in the DLC matrix. Accordingly, the films with high Cr content are characterized by abrasive wear and thus showed a high friction coefficient and wear rate, although they possess a relatively high hardness.

Acknowledgements

The authors are grateful to the financial support of the project of the Natural Science Foundation of China (Grant No: 51072205) and the Science and Technology Department of Zhejiang Province (Grant No: 2008C21055). The authors would like to acknowledge the help provided by Dr. G.S. Wu.

References

[1] Gassner G, Mayrhofer PH, Patscheider J, Mitterer C. Thin Solid Films 2007;515:5411.
[2] Zhang S, Bui XL, Jiang J, Li X. Surf Coat Technol 2005;198:206.
[3] Wang AY, Lee KR, Ahn JP, Han JH. Carbon 2006;44:1826.
[4] Gerhards I, Ronning C, Vetter U, Hofsäss H, Gibhardt H, Eckold G, et al. Surf Coat Technol 2002;158–159:114.
[5] Dub S, Pauleau Y, Thièry F. Surf Coat Technol 2004;180–181:551.
[6] Singh V, Jiang JC, Meletis EI. Thin Solid Films 2005;189:150.
[7] Meng WJ, Tittsworth RC, Rehn LE. Thin Solid Films 2000;377–378:222.
[8] Dai W, Zheng H, Wu GS, Wang AY. Vaccum 2010;85:231.
[9] Zhang HS, Endrino JL, Anders A. Appl Surf Sci 2008;255:2551.
[10] Wilson GM, Saied SO, Field SK. Thin Solid Films 2007;515:7820.
[11] Zhang HS, Komvopoulos K. J Appl Phys 2009;106:093504.
[12] Bewilogua K, Heinitz HJ, Rau B, Schultze S. Thin Solid Films 1988;167:233.
[13] Gulbinski W, Mathur S, Shen H, Suszko T, Gilewicz A, Warcholinski B. Appl Surf Sci 2005;239:302.
[14] Han X, Yan F, Zhang A, Yan P, Wang B, Liu W, et al. Mater Sci Eng A 2003;348:319.